THE JOURNAL OF PHYSICAL CHEMISTRY A
A JOURNAL OF THE AMERICAN CHEMICAL SOCIETY

pubs.acs.org/JPCA Article

Interrogation of O-ATRP Activation Conducted by Singlet and Triplet Excited States of Phenoxazine Photocatalysts

Yisrael M. Lattke, Daniel A. Corbin, Steven M. Sartor, Blaine G. McCarthy, Garret M. Miyake, and Niels H. Damrauer*

Cite This: J. Phys. Chem. A 2021, 125, 3109–3121 Read Online

ACCESS | Metrics & More | Article Recommendations | Supporting Information

ABSTRACT: Organocatalyzed ATRP (O-ATRP) is a growing field exploiting organic chromophores as photoredox catalysts (PCs) that engage in dissociative electron-transfer (DET) activation of alkyl-halide initiators following absorption of light. Characterizing DET rate coefficients (k_{act}) and photochemical yields across various reaction conditions and PC photophysical properties will inform catalyst design and efficient use during polymerization. The studies described herein consider a class of phenoxazine PCs, where synthetic handles of core substitution and *N*-aryl substitution enable tunability of the electronic and spin characters of the catalyst excited state as well as DET reaction driving force (ΔG^0_{ET}). Using Stern–Volmer quenching experiments through variation of the diethyl 2-bromo-2-methylmalonate (DBMM) initiator concentration, collisional quenching is observed. Eight independent measurements of k_{act} are reported as a function of ΔG^0_{ET} for four PCs: four triplet reactants and four singlets with k_{act} values ranging from 1.1×10^8 M^{-1} s^{-1}, where DET itself controls the rate, to 4.8×10^9 M^{-1} s^{-1}, where diffusion is rate-limiting. This overall data set, as well as a second one inclusive of five literature values from related systems, is readily modeled with only a single parameter of reorganization energy under the frameworks of the adiabatic Marcus electron-transfer theory and Marcus–Savéant theory of DET. The results provide a predictive map where k_{act} can be estimated if ΔG^0_{ET} is known and highlight that DET in these systems appears insensitive to PC reactant electronic and spin properties outside of their impact on the driving force. Next, on the basis of measured k_{act} values in selected PC systems and knowledge of their photophysics, we also consider activation yields specific to the reactant spin states as the DBMM initiator concentration is varied. In *N*-naphthyl-containing PCs characterized by near-unity intersystem crossing, the T_1 is certainly an important driver for efficient DET. However, at DBMM concentrations common to polymer synthesis, the S_1 is also active and drives 33% of DET reaction events. Even in systems with low yields of ISC, such as in *N*-phenyl-containing PCs, reaction yields can be driven to useful values by exploiting the S_1 under high DBMM concentration conditions. Finally, we have quantified photochemical reaction quantum yields, which take into account potential product loss processes after electron-transfer quenching events. Both S_1 and T_1 reactant states produce the $PC^{\bullet+}$ radical cation with a common yield of 71%, thus offering no evidence for spin selectivity in deleterious back electron transfer. The subunity $PC^{\bullet+}$ yields suggest that some combination of solvent (DMAc) oxidation and energy-wasting back electron transfer is likely at play and these pathways should be factored in subsequent mechanistic considerations.

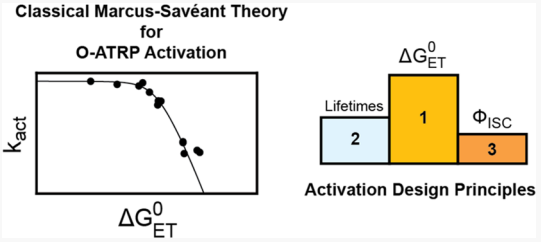

INTRODUCTION

Atom transfer radical polymerization (ATRP)[1,2] is an established method enabling the generation of polymers with narrow molecular-weight distributions and predictable chain lengths that are useful in demanding industrial[3−5] and biomedical[6−8] settings. Polymerization control in ATRP is established through manipulation of two key reaction steps: activation and deactivation. The former occurs when a terminal alkyl-bromide bond on a polymer chain is reductively cleaved by the catalyst to generate a reactive radical on the polymer chain that can grow by propagation. Deactivation is the reverse reaction occurring when a bromide is reinstalled onto the radical polymer chain, thus stopping further growth until subsequent activation. Because of their importance, there have been efforts to modulate the relative rates of activation and deactivation through thermal,[9] electrochemical,[10] sonic,[11] and optical[12,13] means.

Although ATRP is a mature material synthesis methodology, trace contamination from the transition-metal catalysts remains a concern for biomedical and electronic applications,[10,14,15] resulting in a push for metal-free variants as well as methods that allow for ultralow metal-catalyst loading.[16] Organocatalyzed ATRP (O-ATRP) is one such alternative. It exploits

Received: January 29, 2021
Revised: March 23, 2021
Published: April 7, 2021

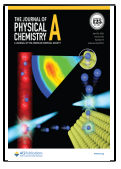

organic chromophores as photoredox catalysts (PCs) that engage in activation following absorption of light. Since the inception of O-ATRP using perylene[17] and *N*-phenylphenothiazine,[18] PC scope has blossomed to include derivatives of phenazine,[19,20] phenoxazine,[21−24] phenothiazine,[25−27] acridine,[28] carbazole,[29] and thienothiophene.[30] Several of these PCs have demonstrated the level of control over a polymerization that is expected from traditional ATRP. The use of light to drive a polymerization further provides many exciting opportunities for spatial and temporal control.[31,32] However, significant additional complexity emerges due to the reliance on photophysical properties and excited-state reactivity. Maturation of this technology requires an understanding of these newly introduced mechanistic details.

The synthetic modularity of many of the organic PC platforms used in O-ATRP has enabled the generation of molecular libraries with diverse properties relevant to photoredox catalysis.[33,34] This modularity includes energetics for critical redox-driven chemical steps, excited-state lifetimes of participatory states, excited-state electronic character such as spin and/or the degree of charge transfer, and the yield with which reactive states are formed.[35] However, it remains unclear how these PC properties impact O-ATRP and specifically how they influence activation and deactivation. In this work, our aim is to contribute to the understanding of how PC properties influence or control activation. We focus on developing a predictive driving force relationship for this process and address the nature in which both electronic and spin characters of excited states are relevant.

In O-ATRP, the necessary driving force for the electron transfer tied to activation comes from the PC being in a photoexcited state. A catalytic cycle (Scheme 1) begins with the absorption of visible light by the ground-state singlet ^{1}PC resulting in the formation of an excited singlet state (^{1}PC*). In competition with its own radiative and nonradiative decay processes, the ^{1}PC* can now either participate directly in activation ($k_{act,S1}$) or, if the rate of intersystem crossing to the triplet state (k_{ISC}) is competitive given the polymerization conditions, form a triplet state (^{3}PC*) that subsequently engages in activation (k_{act,T_1}). Like in metal-catalyzed ATRP, activation is the reductive cleavage of a P_n−Br bond resulting in an activated radical polymer chain, $P_n^\bullet$, the catalyst radical cation, $PC^{\bullet+}$, and a bromide ion, Br^-. The latter two species are anticipated to exist in equilibrium with the association complex $[PC^{\bullet+}Br^-]$.[36] The rest of the catalytic cycle is comparable to the traditional ATRP mechanism. Namely, the active chain $P_n^\bullet$ grows in length (k_{prop}) before it is deactivated by $[PC^{\bullet+}Br^-]$, returning the polymer to its dormant state (P_{n+m}−Br) and regenerating ^{1}PC.

Scheme 1. Proposed O-ATRP Catalytic Cycle[a]

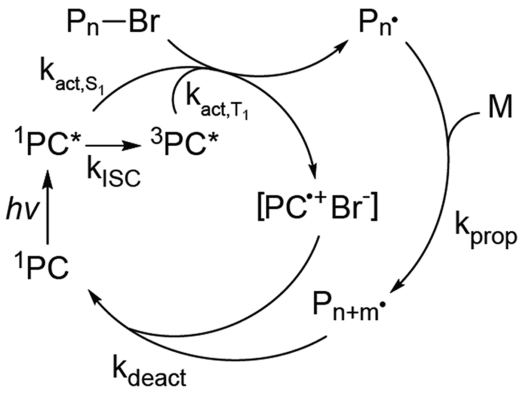

[a]Both the ^{1}PC* and ^{3}PC* can participate in the activation process, with respective rate coefficients k_{act,S_1} and k_{act,T_1}. In both cases, the products of activation are identical.

Whereas k_{act} has been extensively explored in traditional ATRP,[37−39] few values have been reported for O-ATRP. Those values that have been reported indicate that k_{act} can approach values associated with a diffusion-limited process. From these studies,[36,40,41] it has become apparent that there are several unresolved questions regarding how PC molecular properties impact k_{act}. The first concept involves the overarching question of the relationship between the driving force for electron transfer, ΔG^0_{ET}, and the value of k_{act}. Understanding this relationship would enable the prediction of k_{act} in future systems following basic measurements of ground- and excited-state thermodynamic quantities. The second question, which is tied to ΔG^0_{ET}, has to do with whether the singlet or triplet excited state of the PC is the dominant reactant under synthetic conditions. Certainly, high-yield long-lived triplet excited states are commonly desired in solution-phase photoredox catalysis[42] and can be engineered in organic systems without heavy atoms by exploiting molecular substructures with orthogonal π orbitals to increase the spin−orbit coupling and promote intersystem crossing.[43−47] However, the predecessor singlet excited states often have lifetimes on the order of ones to tens of nanoseconds, which can be long enough to engage in bimolecular photochemistry as long as there is sufficient concentration of the reactive partner. The third question involves intramolecular charge-transfer (CT) excited states and the observation that PCs possessing such states perform better in O-ATRP by the metrics of polymer dispersity and initiator efficiency. Because of this observation, there has been discussion[40,48] regarding the relevance or necessity of CT states for expediting forward electron transfer due to a greater degree of coupling for the electron-transfer process. The current work will consider k_{act} from the lens of these three questions.

RESULTS AND DISCUSSION

Photophysical Background. The four phenoxazine PCs **1**−**4** (Figure 1 and Table 1) studied herein were selected for their collective variety in triplet yields (Φ_{ISC}), ΔG^0_{ET}, and degree of excited-state CT character, which will allow us to address each of the three questions mentioned above. Their study yielded eight experimental values of k_{act} by accessing data from the respective lowest-energy ^{1}PC* (i.e., S_1) and ^{3}PC* (i.e., T_1) states. These four PCs have previously been the subject of detailed photophysical investigations,[43,44] and findings in the polar solvent *N*,*N*-dimethylacetamide (DMAc) are summarized here.

Compounds **1** and **2** possess phenyl groups for *N*-aryl substituents, which participate minimally in the photophysics. The S_1 of **1** is almost completely nonpolar and is characterized by a delocalization of charge across the phenoxazine core and both core-phenyl substituents (so-called S_{Deloc}). This state has a 3.24 ns lifetime marked by an efficient fluorescent decay ($\Phi_{em} = k_r/(k_r + k_{nr} + k_{ISC}) = 0.68$) and a moderate yield of intersystem crossing ($\Phi_{ISC} = 0.30$) to a T_1 state characterized by charge transfer from the phenoxazine core to a single core-

https://doi.org/10.1021/acs.jpca.1c00855
J. Phys. Chem. A 2021, 125, 3109−3121

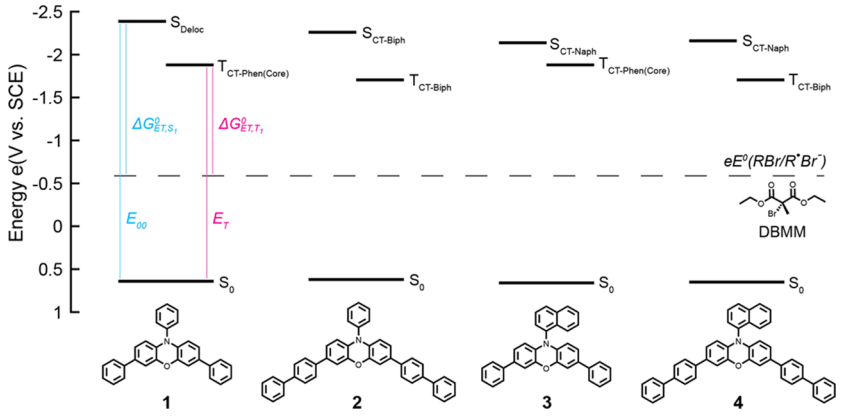

Figure 1. Molecules (PCs **1**−**4** and DBMM) investigated in this study and the energy levels of their ground and excited states expressed on a scale that sets the zero of energy at the energy corresponding to a one-electron reduction requiring 0 V vs saturated calomel electrode (SCE). Greater negative values on this scale represent greater reducing power. The S_0 energy levels correspond to the reduction ($PC^{\bullet+}$/PC), whereas the S_1 and T_1 energy levels are calculated using eq 3 and a modified form of it (eq S6), respectively (see the SI for details and reduction potential values). The dashed line is the energy corresponding to the potential at which DBMM is reduced. The blue and pink lines highlight the quantities used in eq 4 for calculating ΔG^0_{ET}. The small (−47 meV) Coulombic contribution is omitted from the figure.

Table 1. Free Energies for the ET Reaction from S_1 and T_1 States of PCs 1−4 and Associated k_{act} Values

PC	τ_{0,S_1} (ns)	$\Delta G^0_{ET,S_1}$ (eV)	k_{act,S_1} ($\times 10^9$ M^{-1} s^{-1})[a]	Φ_{ISC}	τ_{0,T_1} (ms)	$\Delta G^0_{ET,T_1}$ (eV)	k_{act,T_1} ($\times 10^9$ M^{-1} s^{-1})[b]
1	3.24	−1.87	4.80 ± 0.09	0.30[c]	1.5	−1.34	0.19 ± 0.01
2	2.87	−1.72	3.3 ± 0.3	0.11[d]	1.2	−1.18	0.120 ± 0.009
3	6.32	−1.59	2.0 ± 0.1	0.95[c]	1.5	−1.34	0.20 ± 0.01
4	5.2	−1.62	2.0 ± 0.1	0.91[d]	0.48	−1.16	0.110 ± 0.009

[a]The reported error is twice the standard deviation of a triplicate five-point data set. [b]The reported error comes from the regression analysis of a single 10-point data set (Figure 3). [c]Values from our previous work.[43] [d]Values from our previous work.[44] A detailed table including quantities needed for the calculation of ΔG^0_{ET} is provided in Table S1.

phenyl substituent (so-called $T_{CT\text{-}Phen(core)}$). This T_1 has a lifetime of 1.5 ms. A modification from phenyl core substituents to biphenyl substituents in **2** results in a slight red shift of its maximal wavelength of absorption and an increase in molar absorptivity (see Figure S1). That perturbation also imbues **2** with an S_1 state with partial CT character involving the core and a single biphenyl substituent; it is therefore designated $S_{CT\text{-}Biph}$. This S_1 possesses a 2.87 ns lifetime and decays primarily through radiative means (Φ_{em} = 0.80). With modest yield (Φ_{ISC} = 0.11), it forms a T_1 characterized by charge transfer from the phenoxazine to a single biphenyl substituent, denoted $T_{CT\text{-}Biph}$, with a lifetime of 1.2 ms.

In compounds **3** and **4**, the *N*-aryl substituent is an *N*-naphthyl group. While this has little impact on the absorption spectrum or the nature of the lowest-energy triplet excited states (relative to core-phenyl and core-biphenyl analogues, respectively), it markedly affects other photophysical behaviors. Formed following absorption into the Franck−Condon state, these compounds possess highly polar S_1 states characterized by a charge transfer from the phenoxazine to the orthogonal *N*-naphthyl substituent (so-called $S_{CT\text{-}Naph}$). This electronic character slows radiative decay ($\Phi_{em,3}$ = 0.019 and $\Phi_{em,4}$ = 0.023) while simultaneously speeding intersystem crossing, permitting near-unity Φ_{ISC} in both species ($\Phi_{ISC,3}$ = 0.95 and $\Phi_{ISC,4}$ = 0.91). The S_1 lifetimes of **3** and **4** are 6.32 and 5.2 ns and their T_1 lifetimes are 1.5 and 0.48 ms, respectively.

Measurement of Singlet k_{act} Values. Since the S_1 states in the four species are fluorescent, the shortening or quenching of S_1 lifetimes can be monitored using time-correlated single-photon counting (TCSPC). Quenching experiments were conducted in DMAc using the alkyl-bromide initiator diethyl 2-bromo-2-methylmalonate (DBMM) as a quencher. DMAc and DBMM are commonly used for conducting O-ATRP.

In the absence of a reactive quencher, the singlet lifetime, τ_{0,S_1}, is defined by pathways ascribed to radiative and nonradiative decays, as well as intersystem crossing (eq 1a). In the presence of DBMM, a bimolecular decay pathway is introduced, and the lifetime is shortened (eq 1b)

$$\tau_{0,S_1} = k_{0,S_1}^{-1} = (k_r + k_{nr} + k_{ISC})^{-1} \quad (1a)$$

$$\tau_{S_1} = (k_{act}[DBMM] + k_r + k_{nr} + k_{ISC})^{-1} \quad (1b)$$

Inverting and rearranging eq 1b yields a form of the Stern−Volmer equation[49]

$$\frac{1}{\tau} - \frac{1}{\tau_0} = k_{act}[DBMM] \quad (2)$$

A plot of $\frac{1}{\tau} - \frac{1}{\tau_0}$ data against [DBMM] should exhibit linear growth with a slope equal to the bimolecular rate coefficient, k_{act}, and a zero *y*-intercept. Conducting this analysis results in linear plots with slopes (i.e., k_{act} values) ranging between 2.0×10^9 and 4.80×10^9 M^{-1} s^{-1}. Diffusion places an upper limit on the rate of reaction. In DMAc at 20 °C, the diffusion-limited rate coefficient is estimated to be approximately 6.1×10^9 M^{-1} s^{-1} using a simplified form of the Smoluchowski equation.[50,51] The measured singlet k_{act} values determined from Figure 2 approach this limit but are still sensitive to the excited-state reactant properties.

https://doi.org/10.1021/acs.jpca.1c00855
J. Phys. Chem. A 2021, 125, 3109−3121

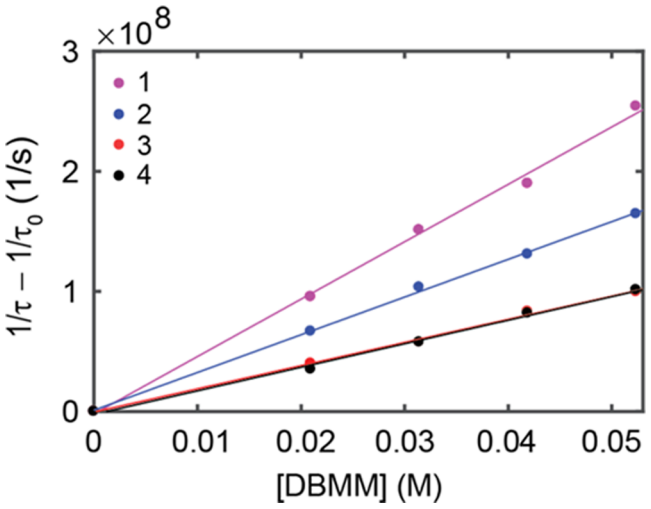

Figure 2. Representative Stern–Volmer plots for S_1 quenching experiments conducted on PCs **1**–**4** and their associated linear fits (solid lines). Each data set comprises five concentration points, including one at [DBMM] = 0 (unquenched). The values and errors presented in Table 1 are the result of triplicate measurements.

Quenching of a singlet excited state is commonly attributed to either energy or electron transfer, but only the latter is expected in our system. Förster resonance energy transfer (FRET) requires spectral overlap between the emission (Figure S1) of the excited-state energy donor and the absorption spectrum of the acceptor. Since there is no absorption signal attributable to DBMM within the UV solvent window of DMAc (268 nm), and the PC emission occurs significantly to the red of 375 nm, FRET is unlikely. Dexter energy transfer would require a dark singlet state for DBMM in resonance with the emitting PC S_1. To the best of our knowledge, there is no reason to suspect that this state is present for this alkyl-halide initiator. Therefore, electron transfer is the quenching pathway. Also, similar systems have been shown to react with alkyl-bromide O-ATRP initiators through dissociative electron transfer, supported by spectroscopic and electron paramagnetic resonance (EPR) studies.[40,41]

The S_1 energy levels in Table 1 combined with redox data can be used to estimate driving forces for excited-state electron transfer. For the free energy available for reductive electron transfer by the S_1 excited-state ^{1}PC*, the following equation is used

$$eE^0(PC^{\cdot+}/\,^1PC^*) = eE^0(PC^{\cdot+}/\,^1PC) - E_{00} \quad (3)$$

Here, e is the fundamental charge, $E^0(PC^{\bullet+}/^1PC)$ is the potential at which the PC radical cation is reduced to the ground-state photocatalyst ^{1}PC, and E_{00} is the free energy stored in ^{1}PC* (measured through a vibronic fitting analysis of the fluorescence spectrum of a given PC—see the SI for details). Once this is known, the driving force for electron transfer to a substrate, ΔG^0_{ET}, can be calculated using eq 4

$$\Delta G^0_{ET} = eE^0(PC^{\cdot+}/PC^*) - eE^0(RX/RX^-) - \frac{e^2}{4\pi\varepsilon_0\varepsilon r} \quad (4)$$

The second term in this equation involves the reduction potential of the alkyl-halide ATRP initiator DBMM leading to the dissociated species. The final term is a Coulombic work term associated with the geminate ion pair (ε_0 is the permittivity of free space, ε is the relative permittivity of the dielectric medium [the solvent], and r is the interionic distance following electron transfer). In the formation of encounter complexes in solution, the distance between reactants that engage in ET often falls between 6 and 10 Å, including a solvation shell.[50−52] For r values within that range, the Coulombic term renders the ET process more exothermic by 37−62 meV (see the SI). While small in magnitude when compared to the rest of the equation, it is important for properly seating driving force values within the greater ET literature. With this consideration in mind, a value of −0.047 eV was chosen, which corresponds to r = 8 Å, an intermediate value of the range quoted above.

All ΔG^0_{ET} values are listed in Table 1, where it is seen that PC **1** has the largest driving force (−1.87 eV). Simultaneously, PC **1** exhibits the most rapid electron transfer of the four PCs with $k_{act} = 4.80 \pm 0.09 \times 10^9$ M^{-1} s^{-1}, nearly at the diffusion-controlled limit. A decrease in the driving force afforded by the lower-energy CT state $S_{CT\text{-}Biph}$ in PC **2** (−1.72 eV) results in a slight decrease of the rate coefficient to $3.3 \pm 0.3 \times 10^9$ M^{-1} s^{-1}, following qualitative expectations of the Marcus theory in the normal regime. PCs **4** and **3** with $S_{CT\text{-}Naph}$ states with even lesser driving force for ET (−1.62 and −1.59 eV) follow this trend and participate in activation at a slower rate, $k_{act} = 2.0 \pm 0.1 \times 10^9$ M^{-1} s^{-1}, for both. While all four PCs can react from their S_1 states, the overall efficacy with which they do so is still in question and will be influenced by the sub-10 ns S_1 lifetimes. We will discuss results relevant to reactivity from the triplet manifold and then discuss the quantum efficiencies associated with both singlet and triplet spin manifolds.

Measurement of Triplet k_{act} Values. The T_1 states of PCs **1**–**4** have sufficient driving forces for ET (Table 1 and Figure 1) as well as lifetimes on the order of milliseconds (vide supra) that are long enough for many potentially productive collisions in solution. However, any one of those collisions should be less productive than a corresponding S_1 state collision due to the lower driving force for ET possessed by the triplet. This reasoning motivates an investigation of reactivity from the T_1 in PCs **1**–**4**, which form in 11–95% efficiency (Table 1) in the absence of a quencher. Prior density functional theory (DFT) studies show that all four T_1 states are CT in character, with the upper singly-occupied molecular orbital (SOMO) residing on a single phenyl (PCs **1**, **3**) or biphenyl core substituent (PCs **2**, **4**) and the lower SOMO on the phenoxazine core, termed $T_{CT\text{-}Phen}$ and $T_{CT\text{-}Biph}$, respectively.[23] *N*-Aryl substitutional differences have a negligible effect on computed T_1 energies (computation of the energy is required because phosphorescence has not been observed) and little effect on the resultant ΔG^0_{ET}. These values as listed in Table 1 are determined using eq 4 and substituting in a DFT-calculated excited-state reduction potential for $E^0(PC^{\bullet+}/^3PC^*)$. In agreement with the predicted orbital characteristics, those PCs sharing common core substituents (**1** with **3** as well as **2** with **4**) have nearly identical excited-state absorption (ESA) features as observed in TA experiments: core-biphenyl PCs **2** and **4** show a maximum in their ESA at 700 nm, and core-phenyl PCs **1** and **3** show an ESA maximum at 650 nm.

We rule out the possibility of triplet energy transfer (TET) from the phenoxazine T_1 state to DBMM being responsible for quenching by appealing to the triplet energies of both reactants. Efficient (diffusion-limited) TET occurs when the

https://doi.org/10.1021/acs.jpca.1c00855
J. Phys. Chem. A 2021, 125, 3109−3121

triplet energy of the donor exceeds that of the acceptor by at least 0.125 eV.[42] DBMM has been sensitized in the past by *p*-anisaldehyde, which possesses a triplet energy of 3.125 eV.[53] In that system, energy transfer to DBMM precedes homolytic cleavage of the R−Br bond, and so, the bond-dissociation energy (BDE) can be taken as a lower bound for the triplet energy. As an estimate, the R−Br BDE for an analogue of DBMM, diethyl 2-bromomalonate, has been measured at 2.75 eV.[54] TET from these phenoxazines (with calculated triplet energies between 2.11 and 2.35 eV) to DBMM is then expected to be endergonic by ∼0.5 eV at the least using the quoted BDE as an estimate, and so, any observed quenching of the triplet states should be attributed to electron transfer.

Stern−Volmer quenching studies were conducted by monitoring lifetime shortening at the ESA of a given T_1 state as a function of [DBMM]. Notably, the DBMM concentration range is approximately three orders of magnitude lower in these experiments compared with that of the singlet studies discussed above, which utilized values closer to common O-ATRP conditions. The four k_{act} values (Table 1) partition into two groups of similar values. PCs **1** and **3**, with core-phenyl substituents, highly similar electronic properties in the T_1, and a common value of $\Delta G^0_{ET} \approx -1.34$ eV, display k_{act} values that are within the error of our measurements at $1.9 \pm 0.1 \times 10^8$ and $2.0 \pm 0.1 \times 10^8$ M^{-1} s^{-1}, respectively. Similarly, PCs **2** and **4** with core-biphenyl substituents with $\Delta G^0_{ET} \approx -1.17$ eV yield k_{act} values of $1.20 \pm 0.09 \times 10^8$ and $1.10 \pm 0.09 \times 10^8$ M^{-1} s^{-1}, respectively. Like the singlet data, the triplet data qualitatively follow the expectations of electron transfer in the Marcus-normal regime, with greater driving forces leading to more rapid electron transfer. In addition to triplet lifetime shortening upon the addition of DBMM, the TA measurements contain a signal associated with the phenoxazine radical cation, which presents as a persistent excited-state absorption signal that does not decay on the time scale of the experiment. Spectroscopic signatures of the radical cation are known from prior spectroelectrochemistry experiments and overlap at all wavelengths that were accessible for measurement of the triplet signals. These observations corroborate the expectation that quenching is due to electron transfer and not to Dexter energy transfer from the PC T_1 (Figure 3).

Driving Force Relationship. Our data (Table 1) span a driving force range of nearly 1 V, over which the corresponding

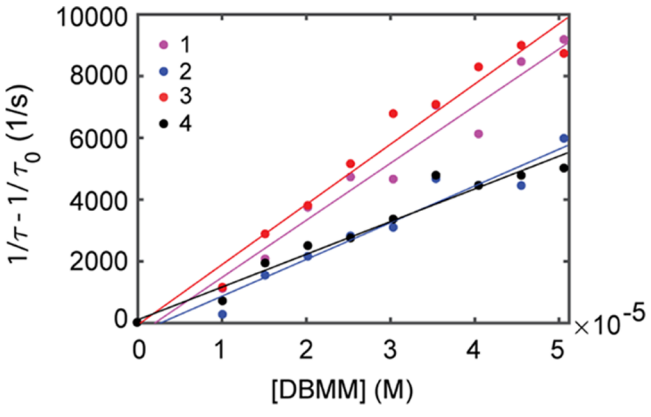

Figure 3. Stern−Volmer plots for T_1 quenching experiments conducted with PCs **1**−**4** and their associated linear fits. Each data set comprises 10 concentration points, including one at [DBMM] = 0 (unquenched).

k_{act} values show a noticeable dependence. We sought to unify these observations in the application of the Marcus theory of electron transfer. The effects of diffusion are explicitly included when considering a bimolecular system since it is a process with a competitive rate coefficient and can have drastic effects on the predicted behavior of the system. Scheme 2 shows the kinetic scheme necessary for describing k_{act}.

Scheme 2. Kinetic Scheme Necessary for Describing k_{act}

$$PC^* + R-Br \underset{k_{-diff}}{\overset{k_{diff}}{\rightleftharpoons}} PC^{*}\cdots R-Br \xrightarrow{k_{ET}} PC^{\bullet+} + R^{\bullet} + Br^-$$

The excited-state PC (irrespective of spin multiplicity) and initiator first diffuse together (k_{diff}) and form an encounter complex. After the encounter complex is generated, it can either break apart (k_{-diff}) or engage in dissociative electron transfer (k_{ET}). The electron-transfer portion of this scheme is simplified to draw focus to the forward electron-transfer process. In the treatment of experimental yields, there are additional processes that need to be considered (vide infra). Within this scheme, the diffusion-limited rate coefficient (k_{diff}) can be estimated using a simplified form[51] of the Smoluchowski equation

$$k_{diff} = \frac{8RT}{3\eta} \tag{5}$$

This equation allows for the estimation of the diffusion-limited rate coefficient in room-temperature DMAc using its viscosity η,[55] the ideal gas constant R, and the temperature T. Using these values produces a value of $k_{diff} = 6.1 \times 10^9$ M^{-1} s^{-1}. The rate coefficient associated with reactants departing, k_{-diff}, is related to k_{diff} through an equilibrium constant:[50−52] $K_d = k_{diff}/k_{-diff}$. For two nonpolar, uncharged reactants such as any of these PC/DBMM pairs that engage in electron transfer with typical encounter distances between 5 and 8.5 Å, K_d is expected to take on values between 0.38 and 1.1 M^{-1} owing to a reliance on the center-to-center distance of the two reactants in the encounter complex—details of this calculation are presented in the SI. Inputting the same center-to-center distance used previously for estimating the Coulombic work term in ΔG^0_{ET}, we estimate $K_d = 0.55$ M^{-1}.

We utilize the classical Marcus theory expression for the electron-transfer rate coefficient, k_{ET}, based on its successful application across a variety of organic dissociative electron-transfer systems, including those that feature aromatic radical anions, transition-metal complexes, and solvated electrons as reductants[50,56]

$$k_{ET} = \frac{k_B T}{h} \exp\left[-\frac{\Delta G^{\ddagger}_{ET}}{k_B T}\right] \tag{6}$$

Equation 6 is the Eyring equation with a unity transmission coefficient ($Z = 1$, not shown) and an activation energy, $\Delta G_{ET}^{\ddagger}$, given by

$$\Delta G^{\ddagger}_{ET} = \frac{(\Delta G^0_{ET} + \lambda_o + BDE)^2}{4(\lambda_o + BDE)} \tag{7}$$

Here, λ_o is the "outer-sphere" reorganizational energy associated with fluctuations of the solvent orientation and polarizability, and BDE refers to the alkyl-halide bond-dissociation energy. In eq 7, the definition of the total

https://doi.org/10.1021/acs.jpca.1c00855
J. Phys. Chem. A 2021, 125, 3109−3121

reorganization energy takes on a form attributed to Savéant in descriptions of the dissociative electron-transfer theory.[57−59] Namely, in the standard Marcus theory, the total reorganization energy is defined as a sum of outer- and inner-sphere contributions ($\lambda = \lambda_o + \lambda_i$), whereas in the Marcus−Savéant theory, the inner-sphere contributions are subsumed in the energetic cost associated with bond cleavage (BDE).

The collective behavior of k_{diff} and k_{ET} can be described by translating Scheme 2 into a set of kinetic equations and applying the steady-state approximation to the encounter complex. In doing this, a composite rate coefficient[60] emerges that connects the quenching rate coefficients determined from Stern−Volmer studies (k_{act}) to the driving force for electron transfer, which is embedded in k_{ET} (via eq 6)

$$k_{act} = \frac{k_{diff}}{1 + \left(\frac{k_{diff}}{K_d}\right)\left(\frac{h}{k_B T}\right)\exp\left[\frac{(\Delta G^0_{ET} + \lambda)^2}{4\lambda k_B T}\right]} \quad (8)$$

A derivation of this formula is provided in the SI.

Figure 4 shows a plot of k_{act} versus ΔG^0_{ET} for the eight data points from compounds **1**−**4** (again, both singlet and triplet

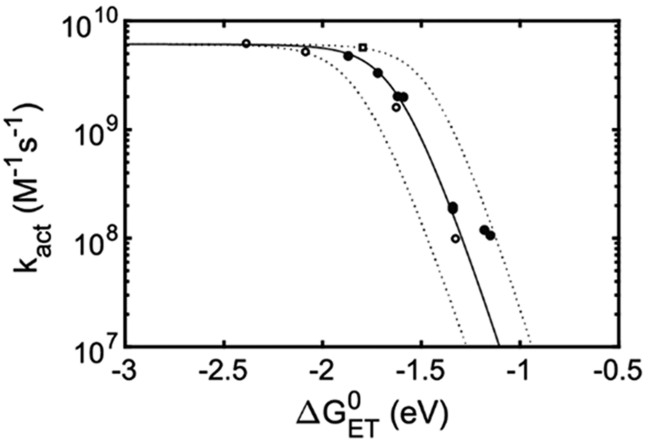

Figure 4. Driving force dependence of k_{act} as observed for our systems (filled circles) as well as values reported by Yagci (hollow circles) and Matyjaszewski (hollow squares). The solid line is a fit of eq 8 to only the data from this work, with K_d = 0.55 M^{-1}, λ = 3.10 eV, and k_{diff} = 6.1 × 10^9 M^{-1} s^{-1}. The dashed lines to either side of the fit indicate the effect of an increase (left) or decrease (right) of the estimated BDE by 10% of its value.

reactivities). Modeling using eq 8 (solid line) is possible with the reorganization energy as a single fitting parameter. Using k_{diff} = 6.1 × 10^9 M^{-1} s^{-1} and K_d = 0.55 M^{-1} as justified previously, we find λ = 3.10 ± 0.02 eV. Also shown in Figure 4 are data from several literature reports of k_{act} including two points with larger ΔG^0_{ET} than is accessible for **1**−**4**. The data points marked by hollow circles correspond to the work by Jockusch and Yagci who measured k_{act} values for quenching of the singlet and triplet states of a phenothiazine-based PC by the alkyl-bromide ATRP initiators methyl α-bromoisobutyrate (MBI) and ethyl α-bromophenylacetate (EBPA) in DMAc.[41] The data point marked by a hollow square comes from Matyjaszewski and co-workers who measured the quenching of a different phenothiazine PC by EBPA.[36] In the case of the full data set (k_{act} for **1**−**4** plus the literature values), fitting indicates λ = 3.09 ± 0.04 eV. It is emphasized that this fit is visually indistinguishable from the fit of the **1**−**4** data set and is not separately included. Overall, the quality of fit to a data set inclusive of rate constants from a significant variety of PCs and quenchers is compelling. Also compelling is the close agreement of λ values when modeling with only data from **1**−**4** versus data from a larger range of ΔG^0_{ET}.

The value of λ = 3.1 eV that we find is of the right magnitude for a dissociative electron transfer in this type of system given that a large portion comes from the alkyl-bromide bond-dissociation energy of DBMM ($\lambda = \lambda_0$ + BDE). The other portion comes from the outer-sphere reorganization energy, for which we assume 0.65 eV. This value is the average of several values estimated by Savéant for dissociative electron transfers involving several alkyl bromides in a similar solvent, *N*,*N*-dimethylformamide (DMF).[57] Using λ_0 = 0.65 eV results in a bond-dissociation energy of 2.45 eV for the R−Br bond in DBMM. This value is similar to a literature value for the alkyl-bromide BDE of DBM, which is 2.75 eV.[54] Additionally, the previously mentioned alkyl-bromide initiators EBPA and MBI have been the subject of a DFT study in which their bond-dissociation energies were calculated at 2.55 and 2.34 eV, respectively.[39] We suspect that a similar study conducted on DBMM would result in an intermediate bond-dissociation energy with respect to the two. MBI has a single adjacent ester group to delocalize the radical across, while the radical formed on EBPA has an adjacent ester and benzene ring. With two adjacent esters, DBMM should act as an intermediate in terms of radical stabilization. The dotted lines in Figure 4 illustrate the expected effects of an increase or decrease of the alkyl-halide BDE by 10% from the estimated value. This range could prove useful for extending the results seen here to systems that employ different initiators and for considering PC-design parameters in those systems.

As a secondary point, it is reiterated that we set out to consider whether there are demonstrable effects of electronic character (for example, the degree of charge transfer) and spin on the dissociative electron-transfer process. Notably, the successful application of the classical Marcus theory (eq 8) argues against this possibility. To further explore this point, the full data set was modeled using a modified version of eq 8 that contains the semiclassical Marcus theory expression for k_{ET} (eq S12a,b) that includes the diabatic electronic coupling V between reactant and product states. In our modeling, the same value of K_d was used, and λ was set to 3.1 eV as determined from the previous classical fitting process. This approach left the electronic coupling as the only fitting coefficient, resulting in a value of V = 25.3 ± 1.5 meV. A value of V that is the same as room-temperature k_BT (25.3 meV at 20 °C) points to a case where adiabatic (classical) theory is appropriate but where semiclassical behavior is not far off. To the former point, Savéant has also observed electronic coupling of similar magnitude with the application of a classical treatment in a dissociative electron-transfer study involving aromatic singlet excited-state reductants and carbon tetrachloride as a dissociative substrate.[61] It is likely that the rate coefficient map of Figure 4 can be applied to many systems. To the latter point, semiclassical considerations may be warranted in cases of significant reactant sterics and a qualitatively different electronic character of the reactant electron donor.

Three regimes of note are present in the Figure 4 data and fits. The first regime is at lower driving forces, for example, between −1 and −1.5 eV, where the triplet k_{act} values from our study lie. In this regime, electron transfer is rate-limiting and the rate constant for diffusion (k_{diff}) has limited impact on k_{act},

https://doi.org/10.1021/acs.jpca.1c00855
J. Phys. Chem. A 2021, 125, 3109−3121

allowing for its estimation to be largely made by appealing to k_{ET} alone: in the limit of $K_d k_{ET} \ll k_{diff}$, then $1 + k_{diff}/K_d k_{ET} \approx k_{diff}/K_d k_{ET}$ and subsequently $k_{act} \approx K_d k_{ET}$ (via eq 8). Here, the largest difference between the fit and data is observed. The measured triplet k_{act} values of PCs **2** and **4** (at the lowest driving force values) are 4−5 times greater than predicted by the fit. This deviation could be a manifestation of a greater electronic coupling for the ET process from those states that have a charge-transfer character. However, more data is needed to further develop this idea. In the current case, the two data points lie in a regime where small changes in driving force, a value estimated using a combination of DFT and electrochemistry (see the SI), have a significant impact on ET rates.

The second regime is in the other driving force extreme, where ΔG^0_{ET} is more negative than −2 eV. Here, $K_d k_{ET} \gg k_{diff}$ and k_{act} approaches diffusion-limited behavior: $k_{act} = k_{diff}$. This phenomenon is known as diffusional leveling, and it is notable that the values included from Jockusch and Yagci pertaining to their phenothiazine's strongly reducing singlet state fall into that second regime. Diffusion control is expected to continue until much greater driving force values, at which point a decrease in rate coefficient associated with entrance into the Marcus inverted regime may be observed.[62] Alternatively, those strongly exoergic electron transfers can lend themselves to the formation of a metastable alkyl-halide radical anion, in which case there are different thermodynamic and kinetic considerations in place, though such discussion is outside the scope of this work.[58,59] The third regime is between the two previous ones, where k_{act} is sensitive to both ET and diffusion. Our study's singlet data sits within this region. Overall, this modeling provides a persuasive retrospective estimation of literature data, including ours, with nearly all values falling within a factor of 2 of the value predicted by the Marcus curve (solid line) in Figure 4. Providing a driving force range map is useful for addressing how a PC excited state, be it singlet or triplet, interacts with the activation process in O-ATRP. Importantly, this map appears useful irrespective of the electronic character (CT, LE) or spin character (singlet, triplet) of the excited-state electron donor.

Competitive Reactivity: Singlets vs Triplets. In the field of O-ATRP, a question is commonly raised as to the nature of the catalytically relevant excited state. In our systems, where photophysical control is engendered by synthetic control of the PC structure, measured k_{act} values can address this concept. PCs **2** and **4** have been chosen for consideration for two reasons. First, they have disparate Φ_{ISC} values of 0.11 vs 0.91, respectively. Second, they have a similar electronic character, as discussed in the Photophysical Background section, characterized as CT in nature involving charge shifting from the phenoxazine core to one of the biphenyl substituents. Thus, a comparison of these species helps to isolate the impact of spin (this comparison is discussed further in the section Conclusions). Irrespective of spin or electronic character of the reactant state, although relying on its lifetime $\tau_0 = (k_0)^{-1}$, the quantum efficiency of activation from an excited state as a function of [DBMM] is written in eq 9A

$$\phi_{act} = \frac{k_{act}[DBMM]}{k_{act}[DBMM] + k_0} \quad (9A)$$

$$\Phi_{act,S_1} = \phi_{act,S_1} \quad (9B)$$

$$\Phi_{act,T_1} = \Phi_{ISC}\phi_{act,T_1} \quad (9C)$$

$$\Phi_{ISC} = \frac{k_{ISC}}{k_{0,S_1} + k_{act}[DBMM]} \quad (9D)$$

For the S_1, which is assumed to be produced in unit quantum yield following light absorption, the overall quantum yield for activation ($\Phi_{act,S1}$) is equivalent to this quantum efficiency of activation (eq 9B). For the T_1, the overall quantum yield for activation ($\Phi_{act,T1}$) must be modified with the yield of intersystem crossing to account for competing non-ET loss processes following light absorption (eq 9C). It is important to recognize that Φ_{ISC} can be thought of as a constant (the value given in Table 1) so long as [DBMM] is low enough that S_1 states will not encounter a quencher molecule. If [DBMM] is sufficiently large that S_1 quenching is expected, Φ_{ISC} will be reduced due to competitive quenching (eq 9D). The quantities $\Phi_{act,S1}$ and $\Phi_{act,T1}$ have been calculated as a function of [DBMM] and are shown for PCs **2** and **4** in Figure 5A,B, respectively. The overlaid green line in the plots shows a commonly employed DBMM concentration for O-ATRP: $[DBMM]_{synth}$ = 45 mM.

As seen by the dashed lines, for both compounds, the T_1 state is the only participant in activation at values of [DBMM] below 1 mM. This role maximizes with a yield of activation almost equivalent to the respective unquenched Φ_{ISC} before decreasing due to the onset of singlet-state reactivity, which competes with the intersystem crossing process (see eq 9D).

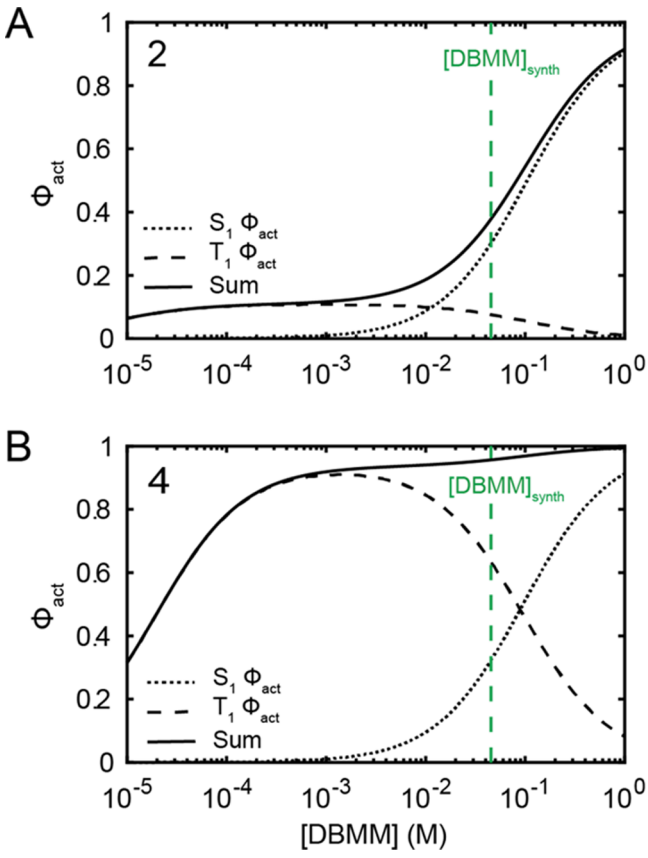

Figure 5. Semilogarithmic plots of the calculated (eq 9A−9A) quantum yields of activation from the S_1 state, T_1 state, and the sum of the two for PCs **2** (A) and **4** (B) as a function of [DBMM]. PC **2**'s low predicted yield at lower values of DBMM reflects its poor ability to form its long-lived T_1, while the near-unity triplet yield of **4** engenders it with uniform reactivity over a large concentration range.

https://doi.org/10.1021/acs.jpca.1c00855
J. Phys. Chem. A 2021, 125, 3109−3121

For **2**, which was chosen because of its low Φ_{ISC}, a turnover in reactive-state identity occurs at about 10 mM, after which S_1 reactivity is the more important consideration. For **4**, given its near-unity Φ_{ISC}, O-ATRP activation is expected to be efficient even at 10−100 μM concentrations of initiator. This efficiency continues to increase as initiator is added and by $[DBMM]_{synth}$ activation is nearly quantitative. At that concentration, the T_1 is expected to be responsible for twice as many activation reactions as the S_1, making it the major catalytic state for PC **4** under synthetic conditions. It is important to note that even at $[DBMM]_{synth}$ this is not the case with PC **2**, which is primarily reactive from its S_1 due to its poor Φ_{ISC}. Because of this, much greater [DBMM] would be necessary for PC **2** to achieve the same total activation efficiency of PC **4**. While high Φ_{ISC} is a promoter of the T_1 state reactivity, it is important to recognize that the S_1 reactivity should not be ignored. While there are certainly differences in the reactive behavior of the two photocatalysts, there is not massive disparity in the proportion of state reactivity at $[DBMM]_{synth}$: T_1 versus S_1 reactivity occurs with a ratio of 1:4 and 2:1 for **2** and **4**, respectively. An analogous result comes from conducting this analysis on PCs **1** and **3**, which have similar relative Φ_{ISC} values to **2** and **4**.

Photochemical Quantum Yield of Dissociative Electron Transfer. While Figure 5 is compelling for understanding origins of reactivity under various reaction conditions, it is based on observations of electron-transfer quenching and ultimately does not speak to the possibility of spin-state dependencies in photochemical product yield arising because of competition with nonproductive pathways such as back electron transfer. In this section, we address this question and describe experiments to measure the quantum yield of productive dissociative electron transfer to form the fragmented products ($PC^{\bullet+}$, $R^{\bullet}$, and Br^{-}).

Photochemical quantum yields are measured from the vantage point of ground-state species as a ratio of the moles of photoproduct generated over a period of illumination with the moles of photons absorbed over that same period

$$\Phi_{rxn} = \frac{\text{moles of photoproduct formed}}{\text{moles of photons absorbed}} \tag{10}$$

The kinetics of a photoreaction can be complicated; however, they are simplified and forced into a zeroth-order regime (see the SI for an extensive discussion, including kinetic simulations of the system) when the concentration of the absorbing species is large enough that more than 99% of the photons incident on the reaction mixture are absorbed.[63−65] In general, the rate of photon absorption at a specific wavelength, $W(\lambda)$, can be written as

$$W(\lambda) = I_0(\lambda)(1 - 10^{-A(\lambda)}) \tag{11}$$

where $I_0(\lambda)$ is the intensity of the excitation light with wavelength λ incident on the reaction mixture, and $A(\lambda)$ is the photoreactant absorbance at that same wavelength. In the high-absorbance limit (typically taken to be $A > 2$), eq 11 simplifies since the exponential term can be omitted, resulting in $W(\lambda) = I_0(\lambda)$. Hence, so long as the sample absorbance fits this criterion, the moles of photons absorbed over a certain time period can be calculated as $I_0(\lambda)t$, so long as the intensity $I_0(\lambda)$ is known. This intensity measurement can be conducted with a calibrated power meter or with a chemical actinometer. We opted for the former and detail that measurement in the SI.

The most straightforward means of observing photoproduct generation in these systems is via the absorption signal of the generated PC radical cation, which exhibits multiple bright absorption bands in the visible spectrum (Figure 6). The

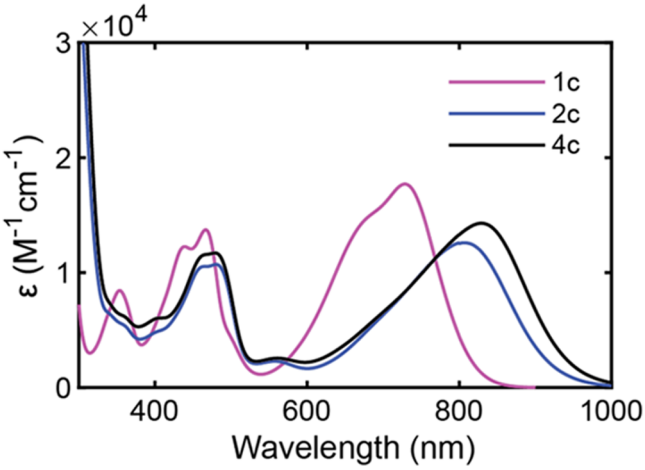

Figure 6. Absorption spectra of the radical cation hexafluorophosphate salts, collected in MeCN, scaled to their peak molar attenuation coefficients. Beer's law studies are presented in the SI.

radical cation concentration, [*c*], can in principle be calculated given an absorbance measurement at a wavelength devoid of a signal from other species. Initial attempts were made using spectroelectrochemical conversion to determine the spectra and corresponding molar attenuation coefficients for the radical cations in DMAc. However, these measurements proved intractable due to incomplete transformation from PC to $PC^{\bullet+}$ within the spectroscopic volume. The radical cations show a propensity for loss by oxidation of DMAc in the dark and more rapidly upon illumination. To overcome this challenge, we identified acetonitrile as a more oxidatively stable solvent with a comparable dielectric constant to DMAc and turned to chemical methods for quantitative generation of radical cations **1c**, **2c**, and **4c** (synthetic details in the SI). With these bench-stable radical cations in hand, molar attenuation coefficient values were measured for all three compounds via a Beer's law study (see the SI). The absorption spectra (Figure 6) of **2c** and **4c**, which both contain biphenyl core substituents, are quite similar possessing a dominant, broad, near-IR peak centered at 808 nm ($\varepsilon_{808,2c}$ = 12 600 cm^{-1} M^{-1}) and 830 nm ($\varepsilon_{830,4c}$ = 14 300 cm^{-1} M^{-1}), respectively, and a less intense bluer feature that peaks near 480 nm. The spectrum for **1c** shows certain similarities to **2c** and **4c**, although features are blue-shifted owing to the smaller aromatic core substituents. A broad intense band peaks at 728 nm ($\varepsilon_{728,1c}$ = 17 700 cm^{-1} M^{-1}), and there is a double-peaked band near 450 nm. Additionally, a band at 360 nm is resolved for **1c**, which is in a similar position to that of the parent PC. Because the lowest-energy absorption peaks of the radical cations do not overlap with absorption or emission signatures of the respective parent PCs (see Figure S1), they permit observations that can be ascribed purely to product generation during a photoreaction.

As noted earlier and illustrated in Figure 5, the choice of the PC system and initiator concentration allows us to control reactant qualities such as the spin state engaged in photochemistry. We first target quantification of a reaction quantum yield involving singlet reactivity by considering PC **2** with a

https://doi.org/10.1021/acs.jpca.1c00855
J. Phys. Chem. A 2021, 125, 3109−3121

high DBMM concentration of 1 M. Figure 7A illustrates the growth of the absorption spectrum of **2c** over an irradiation

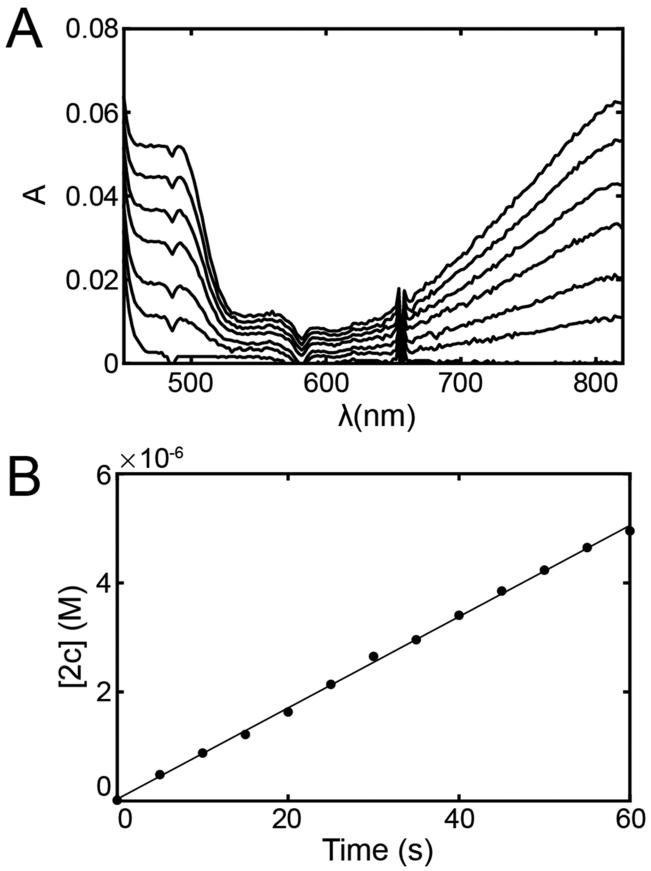

Figure 7. (A) Growth of the absorption signal of **2c** over time in a photoreaction. (B) Kinetic trace at 816 nm converted to [**2c**] via Beer's law, with a linear fit demonstrating its zeroth-order kinetic behavior.

period of 60 s. The corresponding plot of [**2c**] vs t (Figure 7B) shows the linear growth expected from forcing this photoreaction into a zeroth-order kinetic regime. The slope (m) of the linear fit to this data gives the rate of [**2c**] generation in units of M s^{-1}. As mentioned previously, at sufficiently high absorbances, the rate of photon absorption (in units of M s^{-1}) is constant and so the total number of photons absorbed over a period (t) is given by I_0t. Thus, the quantum yield of radical cation generation (i.e., eq 10: (mols of photoproduct)/(mols of photons absorbed)) can be determined as

$$\Phi_{rxn} = \frac{mt}{I_0 t} = \frac{m}{I_0} \tag{12}$$

We find for **2** a value of Φ_{rxn} = 0.64 ± 0.04 (Table 2).

Because the quantity Φ_{rxn} is referenced relative to ground-state species that absorb light and not relative to the specific states performing the dissociative electron transfer, it is important to take a step further and quantify the reaction yield in a way that accounts for competing photophysical and/or photochemical pathways. In a general way, we can write in eq 13A that the quantum yield of reaction can be broken into a product of the quantum yield for activation (Φ_{act})—where activation is thought of as the bimolecular quenching phenomenon—and the yield of productive dissociative electron transfer that generates an observed radical cation

Table 2. Values Related to the Measurement of Photochemical Quantum Yields

PC	λ_{max} (nm) for $PC^{\bullet+}$ [a]	$\varepsilon_{\lambda_{max}}$ (M^{-1} cm^{-1}) [a]	Φ_{act} [b]	Φ_{rxn} [c]	Φ_{+} [d]
1	728	17 700 ± 600	0.94	0.42 ± 0.05	0.45 ± 0.05
2	808	12 600 ± 400	0.90	0.64 ± 0.04	0.71 ± 0.04
4	830	14 300 ± 900	1.0	0.65 ± 0.02	0.71 ± 0.07

[a]In MeCN, error bars come from the regression analysis of Beer's law plots. [b]Calculated using eq 9A–9D with [DBMM] = 1 M for **1** and **2**, and 1 mM for **4**. [c]Error bars calculated as twice the standard deviation from three separate measurements. [d]For PC **4**, this was calculated using the previously measured value of Φ_{ISC} (0.91; Table 1). The error bars come from propagating the error of the individual measurements.

(Φ_{+}). In this way, it is seen that the reaction yield depends not only on the quenching events carried out in Φ_{act} but also on how the excited-state reactant enables the production of the radical cation product

$$\Phi_{rxn} = \Phi_{act}\Phi_{+} \tag{13A}$$

$$\Phi_{+,S_1} = \Phi_{rxn,S_1}/\Phi_{act,S_1} = \Phi_{rxn,S_1}/\phi_{act,S_1} \tag{13B}$$

$$\Phi_{+,T_1} = \Phi_{rxn,T_1}/\Phi_{act,T_1} = \Phi_{rxn,T_1}/\Phi_{ISC}\phi_{act,T_1} \tag{13C}$$

Then, by appealing to eqs 9B and 9C, we can write reaction yield expressions that are specific to the states engaging in them. For **2** under high [DBMM] conditions, the specific state engaging in the photochemistry is the S_1 and we appeal to eq 13B. The quantum yield of S_1 formation is unity; however, electron transfer is in meaningful competition with radiative decay such that at 1 M DBMM, $\Phi_{act,S_1} = \phi_{act,S_1}$ = 0.9 (Table 2). Thus, it is found that Φ_{+,S_1} = 0.71 ± 0.04.

Turning to a triplet excited-state reactor in **4** at 1 mM DBMM, we again find linear growth in **4c** (Figure S8C) and using eq 12, we find a remarkably similar $\Phi_{rxn,T1}$ = 0.65 ± 0.02 (Table 2). Given that Φ_{ISC} is not unity (it is 0.91; Table 1), but recognizing that the quantum efficiency of activation for this state once formed is unity ($\phi_{act,T1}$; eq 9A), we find $\Phi_{+,T1}$ = 0.71 ± 0.07 (Table 2), an identical finding to that of the PC **2**'s S_1. This finding is highly notable given that the electronic character of the T_1 in **4** is expected to be the same as the S_1 in **2**, with CT manifesting from the phenoxazine core to one of the biphenyl substituents (vide supra).

Thus, to the extent that we have controlled for and eliminated complications from electronic or other unforeseen factors, we can conclude that there is no spin dependence on productive dissociative electron transfer. As the forward electron transfer event is manifest in the events of quenching and quantified with Φ_{act}, this current finding in Φ_{+} suggests no meaningful spin dependence in subsequent events that compete with photoproduct formation. Potentially competing events include (a) DMAc oxidation by $PC^{\bullet+}$, which we know to be operative, albeit yet unquantified, from our spectroelectrochemical studies (vide supra) and (b) back electron-transfer events wherein the photoproducts $PC^{\bullet+}$, $R^{\bullet}$ (the DBMM initiator following halide loss), and Br^{-} recombine to generate singlet ground-state species PC and DBMM. Because the one-electron reduction potentials[23] ($PC^{\bullet+}$/PC) are nearly identical for **2** and **4**, we can conclude that there is no evidence for spin-dependent loss via back electron transfer. It is noted that

https://doi.org/10.1021/acs.jpca.1c00855
J. Phys. Chem. A 2021, 125, 3109–3121

Φ_{rxn,S_1} was also measured for **1**, as shown in Table 2. This system is discussed in the Conclusions section.

CONCLUSIONS

In this work, we have measured rate coefficients for dissociative electron transfer k_{act} for a set of PCs whose structural control through core and *N*-substitution enables manipulation of reactant-state electronic structure, spin, and driving force (ΔG^0_{ET}) in reacting with the alkyl-halide initiator DBMM. Additionally, we have quantified reaction yields for the formation of $PC^{\bullet+}$ photoproducts. From this, we draw three sets of interrelated conclusions.

First, we find that the adiabatic Marcus theory of electron transfer is appropriate for modeling the relationship between k_{act} and ΔG^0_{ET} for a significant number of systems of varied reactant spin and electronic characters. This suggests that the diabatic coupling between reactant and product states is large, on the order of k_BT, which is likely a manifestation of significant interactions between the PC π^* system populated in the S_1 and T_1 states and antibonding orbitals in the initiator affecting its C−Br bond. The efficacy of a general model, with the inference of there being an average electronic coupling relevant for many types of reactant/DBMM combinations, suggests that in these types of systems, i.e., phenoxazines or perhaps more generally chromophores with open and accessible π systems, there may be limited value in seeking designs on the sole basis of a reactant excited-state electronic structure such as CT versus LE states. Rather, the focus should be on the driving force, pushing toward diffusion-limited ET behavior, and/or extending the inherent PC lifetimes, which extends the likelihood of encountering initiator while limiting competition from loss pathways. Discussed a different way, it may be inferred that the measured photophysical behavior and thermodynamics of new PCs may be sufficient information when coupled with the Marcus curve of Figure 4 to predict rate coefficients for DET.

A second set of conclusions follows from the fact that measured k_{act} values in concert with the photophysical knowledge of the PCs allows for modeling of activation (DET) yield as the DBMM concentration is varied. Importantly, this can now be visualized as a function of which reactant spin state (S_1 or T_1) is engaging in the photochemistry. For PC **4**, where ISC is high yielding, T_1 reactivity is dominant at low [DBMM]. However, S_1 reactivity remains relevant owing to its greater driving force resulting in its larger k_{act}. Under common synthetic conditions for [DBMM], S_1 reactivity accounts for 33% of DET within an overall yield that is nearly quantitative at 96%. By the same token, systems such as PC **2** that exhibit low ISC yields but significant driving force from their S_1 state can still be successful photocatalysts, even with short lifetimes. At synthetic [DBMM], the overall activation yield for **2** is lessened compared to that for **4** but it is still 40%, with 80% of that overall yield coming from the S_1. Significant S_1 activation yield improvements are possible for systems with modest increases in lifetime. For example, a PC with the driving force of PC **2** and a 20 ns S_1 lifetime would yield 75% driven from the S_1 alone at the polymerization-relevant initiator concentration. Some caution is warranted regarding exploitation of the S_1 in O-ATRP. As solution viscosity increases due to polymer growth, diffusion slows, and the advantages of high driving force will be muted with the reaction time. Exploitation of primarily S_1-reacting PCs may need to focus on low-viscosity (i.e., common solvents used in synthesis) settings/applications. In photocatalytic cycles where DET is relevant for small-molecule activation and not polymer growth, this will not be an issue. While this study casts PCs **1**−**4** as reductants for DET, their ample S_1 and T_1 excited-state reduction potentials should ensure diffusion-limited ET in systems where bond-breaking does not factor into the reorganization energy cost.

Finally, a third set of conclusions centers on the measurement of photochemical reaction yields as determined by observation of the $PC^{\bullet+}$ product. This is a significant step beyond treating activation alone because it addresses yields of fragmented DET products, which have successfully avoided potential loss pathways such as back electron transfer (deactivation) following the initial ET event. In other words, even while activation yields are valuable and suggestive, there is no guarantee that forward ET results in the observation of fragmented products. In studies of **4** and **2** under reaction conditions that isolate T_1 versus S_1 reactivity, respectively, we observe identical reaction yields of 64%. Factoring spin-state-specific loss or formation pathways, it is shown that the S_1 of **2** and the T_1 of **4**, which possess a similar SOMO character, produce $PC^{\bullet+}$ with an identical 71% yield. This suggests that the reactant spin in these systems does not impact photochemical yield.

There are two reasonable factors contributing to subunity $PC^{\bullet+}$ formation. The first is back electron transfer leading to reformation of the alkyl-halide bond and reduction of $PC^{\bullet+}$. The absence of an observed spin dependence on the photoreaction quantum yield is not unreasonable as one could imagine that there is enough time prior to back electron transfer for dephasing of the spin centers on the alkyl radical and the $PC^{\bullet+}$. The second is simple solvent oxidation by $PC^{\bullet+}$ (or photoexcited $PC^{\bullet+}$) once it is formed by either spin pathway, leading to cation loss and formation of ground-state PC. Such an oxidation would be useful by way of reforming the photocatalyst, but the potential mechanistic role of the nascent solvent radical is unknown and interesting.

Related to this question of solvent oxidation, we point to the measured photochemical quantum yield for **1** with a value of 42% associated with the S_1 reactant (seen in Table 2). This is notably smaller than that seen for **2** (also an S_1 reactor) or **4** (a T_1 reactor with a similar CT-biphenyl character), where a yield of 64−65% was observed. In the possible limit that solvent oxidation is not a factor, one might be seeing evidence that a CT reactant state (**2** or **4**) achieves a higher reaction yield than nonpolar core-delocalized state (**1**). Since there appears to be no clear mechanistic difference for the forward ET process, this might then indicate that electronic differences can affect loss pathways via back ET, perhaps by way of solvent reorganization effects. However, because **1c** is a stronger oxidant than **2c** or **4c**, solvent oxidation may as well be the origin of the yield disparity. Photochemical yield experiments in more oxidatively stable environments are needed to address these issues, and experiments along these lines are being considered in the ongoing work.

ASSOCIATED CONTENT

Supporting Information

The Supporting Information is available free of charge at https://pubs.acs.org/doi/10.1021/acs.jpca.1c00855.

https://doi.org/10.1021/acs.jpca.1c00855
J. Phys. Chem. A 2021, 125, 3109−3121

Chemical information, absorption and emission data, photophysical methods and sample preparation, cyclic voltammetry, bimolecular Marcus theory details, excited-state reduction potential calculations and driving force calculations, error analysis for triplet quenching data, k_{diff} estimation, K_d estimation, semiclassical Marcus theory k_{act} expression, photoreaction kinetics exploration, photochemical quantum yield experimental details, synthesis/characterization of radical cations, and Beer's law studies for radical cations (PDF)

AUTHOR INFORMATION

Corresponding Author

Niels H. Damrauer − *Department of Chemistry, University of Colorado, Boulder, Colorado 80309, United States;* orcid.org/0000-0001-8337-9375; Email: Niels.Damrauer@Colorado.edu

Authors

Yisrael M. Lattke − *Department of Chemistry, University of Colorado, Boulder, Colorado 80309, United States*

Daniel A. Corbin − *Department of Chemistry, Colorado State University, Fort Collins, Colorado 80523, United States*

Steven M. Sartor − *Department of Chemistry, University of Colorado, Boulder, Colorado 80309, United States*

Blaine G. McCarthy − *Department of Chemistry, Colorado State University, Fort Collins, Colorado 80523, United States*

Garret M. Miyake − *Department of Chemistry, Colorado State University, Fort Collins, Colorado 80523, United States;* orcid.org/0000-0003-2451-7090

Complete contact information is available at: https://pubs.acs.org/10.1021/acs.jpca.1c00855

Notes

The authors declare no competing financial interest.

ACKNOWLEDGMENTS

The authors would like to thank Prof. Gordana Dukovic for providing access to her TCSPC instrument and her graduate students Jesse L. Ruzicka and Dr. Orion M. Pearce for training. Dr. Pearce also participated in many fruitful discussions regarding the interpretation of quenching results. The authors thank Prof. Josef Michl and his graduate student Andrew Chomas for lending them the mounted LED and driver employed in the measurement of photoreaction quantum yields. This work was supported by the National Science Foundation under Award no. 2016557 and by the National Institutes of Health under Award no. R35GM119702. The content is solely the responsibility of the authors and does not necessarily represent the official views of the National Institutes of Health. S.M.S. and B.G.M. are grateful for support from NSF GRFPs. Y.M.L. acknowledges support from the Department of Education under a GAANN fellowship.

REFERENCES

(1) Kato, M.; Kamigaito, M.; Sawamoto, M.; Higashimura, T. Polymerization of Methyl Methacrylate with the Carbon Tetrachloride/Dichlorotris-(Triphenylphosphine)Ruthenium(II)/Methylaluminum Bis(2,6-Di-Tert-Butylphenoxide) Initiating System: Possibility of Living Radical Polymerization. *Macromolecules* **1995**, *28*, 1721−1723.

(2) Wang, J.-S.; Matyjaszewski, K. Controlled/"Living" Radical Polymerization. Atom Transfer Radical Polymerization in the Presence of Transition-Metal Complexes. *J. Am. Chem. Soc.* **1995**, *117*, 5614−5615.

(3) Matyjaszewski, K.; Spanswick, J. Controlled/Living Radical Polymerization. *Mater. Today* **2005**, *8*, 26−33.

(4) Camenzind, H.; Dubs, P.; Hänggi, P.; Martin, R.; Mühlebach, A.; Rime, F. Polymers Produced by Atom Transfer Radical Polymerisation Technique with Structurally Modified Terminal Groups. Google Patents WO2003/095512, 2009.

(5) Auschra, C.; Eckstein, E.; Mühlebach, A.; Zink, M.-O.; Rime, F. Design of New Pigment Dispersants by Controlled Radical Polymerization. *Prog. Org. Coat.* **2002**, *45*, 83−93.

(6) Bencherif, S. A.; Washburn, N. R.; Matyjaszewski, K. Synthesis by AGET ATRP of Degradable Nanogel Precursors for in Situ Formation of Nanostructured Hyaluronic Acid Hydrogel. *Biomacromolecules* **2009**, *10*, 2499−2507.

(7) Oh, J. K.; Bencherif, S. A.; Matyjaszewski, K. Atom Transfer Radical Polymerization in Inverse Miniemulsion: A Versatile Route toward Preparation and Functionalization of Microgels/Nanogels for Targeted Drug Delivery Applications. *Polymer* **2009**, *50*, 4407−4423.

(8) Oh, J. K.; Siegwart, D. J.; Matyjaszewski, K. Synthesis and Biodegradation of Nanogels as Delivery Carriers for Carbohydrate Drugs. *Biomacromolecules* **2007**, *8*, 3326−3331.

(9) Konkolewicz, D.; Magenau, A. J. D.; Averick, S. E.; Simakova, A.; He, H.; Matyjaszewski, K. ICAR ATRP with Ppm Cu Catalyst in Water. *Macromolecules* **2012**, *45*, 4461−4468.

(10) Magenau, A. J. D.; Strandwitz, N. C.; Gennaro, A.; Matyjaszewski, K. Electrochemically Mediated Atom Transfer Radical Polymerization. *Science* **2011**, *332*, 81−84.

(11) Mohapatra, H.; Kleiman, M.; Esser-Kahn, A. P. Mechanically Controlled Radical Polymerization Initiated by Ultrasound. *Nat. Chem.* **2017**, *9*, 135.

(12) Kwak, Y.; Matyjaszewski, K. Photoirradiated Atom Transfer Radical Polymerization with an Alkyl Dithiocarbamate at Ambient Temperature. *Macromolecules* **2010**, *43*, 5180−5183.

(13) Fors, B. P.; Hawker, C. J. Control of a Living Radical Polymerization of Methacrylates by Light. *Angew. Chem., Int. Ed.* **2012**, *51*, 8850−8853.

(14) Mueller, L.; Matyjaszewski, K. Reducing Copper Concentration in Polymers Prepared via Atom Transfer Radical Polymerization. *Macromol. React. Eng.* **2010**, *4*, 180−185.

(15) Matyjaszewski, K. Atom Transfer Radical Polymerization (ATRP): Current Status and Future Perspectives. *Macromolecules* **2012**, *45*, 4015−4039.

(16) Corrigan, N.; Jung, K.; Moad, G.; Hawker, C. J.; Matyjaszewski, K.; Boyer, C. Reversible-Deactivation Radical Polymerization (Controlled/Living Radical Polymerization): From Discovery to Materials Design and Applications. *Prog. Polym. Sci.* **2020**, *111*, No. 101311.

(17) Miyake, G. M.; Theriot, J. C. Perylene as an Organic Photocatalyst for the Radical Polymerization of Functionalized Vinyl Monomers through Oxidative Quenching with Alkyl Bromides and Visible Light. *Macromolecules* **2014**, *47*, 8255−8261.

(18) Treat, N. J.; Sprafke, H.; Kramer, J. W.; Clark, P. G.; Barton, B. E.; Read de Alaniz, J.; Fors, B. P.; Hawker, C. J. Metal-Free Atom Transfer Radical Polymerization. *J. Am. Chem. Soc.* **2014**, *136*, 16096−16101.

(19) Theriot, J. C.; Lim, C.-H.; Yang, H.; Ryan, M. D.; Musgrave, C. B.; Miyake, G. M. Organocatalyzed Atom Transfer Radical Polymerization Driven by Visible Light. *Science* **2016**, *352*, 1082−1086.

(20) Cole, J. P.; Federico, C. R.; Lim, C.-H.; Miyake, G. M. Photoinduced Organocatalyzed Atom Transfer Radical Polymerization Using Low Ppm Catalyst Loading. *Macromolecules* **2019**, *52*, 747−754.

(21) Du, Y.; Pearson, R. M.; Lim, C.-H.; Sartor, S. M.; Ryan, M. D.; Yang, H.; Damrauer, N. H.; Miyake, G. M. Strongly Reducing, Visible-Light Organic Photoredox Catalysts as Sustainable Alternatives to Precious Metals. *Chem. - Eur. J.* **2017**, *23*, 10962−10968.

(22) Pearson, R. M.; Lim, C. H.; McCarthy, B. G.; Musgrave, C. B.; Miyake, G. M. Organocatalyzed Atom Transfer Radical Polymer-

ization Using N-Aryl Phenoxazines as Photoredox Catalysts. *J. Am. Chem. Soc.* **2016**, *138*, 11399−11407.
(23) McCarthy, B. G.; Pearson, R. M.; Lim, C.-H.; Sartor, S. M.; Damrauer, N. H.; Miyake, G. M. Structure−Property Relationships for Tailoring Phenoxazines as Reducing Photoredox Catalysts. *J. Am. Chem. Soc.* **2018**, *140*, 5088−5101.
(24) Park, G. S.; Back, J.; Choi, E. M.; Lee, E.; Son, K. Visible Light-Mediated Metal-Free Atom Transfer Radical Polymerization with N-Trifluoromethylphenyl Phenoxazines. *Eur. Polym. J.* **2019**, *117*, 347−352.
(25) Discekici, E. H.; Anastasaki, A.; Read de Alaniz, J.; Hawker, C. J. Evolution and Future Directions of Metal-Free Atom Transfer Radical Polymerization. *Macromolecules* **2018**, *51*, 7421−7434.
(26) Dadashi-Silab, S.; Pan, X.; Matyjaszewski, K. Phenyl Benzo-[b]Phenothiazine as a Visible Light Photoredox Catalyst for Metal-Free Atom Transfer Radical Polymerization. *Chem. - Eur. J.* **2017**, *23*, 5972−5977.
(27) Corbin, D. A.; Lim, C.-H.; Miyake, G. M. Phenothiazines, Dihydrophenazines, and Phenoxazines: Sustainable Alternatives to Precious-Metal-Based Photoredox Catalysts. *Aldrichimica Acta* **2019**, *52*, 7.
(28) Buss, B. L.; Lim, C.-H.; Miyake, G. M. Dimethyl Dihydroacridines as Photocatalysts in Organocatalyzed Atom Transfer Radical Polymerization of Acrylate Monomers. *Angew. Chem., Int. Ed.* **2020**, *59*, 3209−3217.
(29) Huang, Z.; Gu, Y.; Liu, X.; Zhang, L.; Cheng, Z.; Zhu, X. Metal-Free Atom Transfer Radical Polymerization of Methyl Methacrylate with Ppm Level of Organic Photocatalyst. *Macromol. Rapid Commun.* **2017**, *38*, No. 1600461.
(30) Kutahya, C.; Allushi, A.; Isci, R.; Kreutzer, J.; Ozturk, T.; Yilmaz, G.; Yagci, Y. Photoinduced Metal-Free Atom Transfer Radical Polymerization Using Highly Conjugated Thienothiophene Derivatives. *Macromolecules* **2017**, *50*, 6903−6910.
(31) Corrigan, N.; Yeow, J.; Judzewitsch, P.; Xu, J.; Boyer, C. Seeing the Light: Advancing Materials Chemistry through Photopolymerization. *Angew. Chem., Int. Ed.* **2019**, *58*, 5170−5189.
(32) Jung, K.; Corrigan, N.; Ciftci, M.; Xu, J.; Seo, S. E.; Hawker, C. J.; Boyer, C. Designing with Light: Advanced 2D, 3D, and 4D Materials. *Adv. Mater.* **2020**, *32*, No. 1903850.
(33) Corrigan, N.; Shanmugam, S.; Xu, J.; Boyer, C. Photocatalysis in Organic and Polymer Synthesis. *Chem. Soc. Rev.* **2016**, *45*, 6165−6212.
(34) Lee, Y.; Kwon, M. S. Emerging Organic Photoredox Catalysts for Organic Transformations. *Eur. J. Org. Chem.* **2020**, *2020*, 6028−6043.
(35) Singh, V. K.; Yu, C.; Badgujar, S.; Kim, Y.; Kwon, Y.; Kim, D.; Lee, J.; Akhter, T.; Thangavel, G.; Park, L. S.; et al. Highly Efficient Organic Photocatalysts Discovered via a Computer-Aided-Design Strategy for Visible-Light-Driven Atom Transfer Radical Polymerization. *Nat. Catal.* **2018**, *1*, 794−804.
(36) Pan, X.; Fang, C.; Fantin, M.; Malhotra, N.; So, W. Y.; Peteanu, L. A.; Isse, A. A.; Gennaro, A.; Liu, P.; Matyjaszewski, K. Mechanism of Photoinduced Metal-Free Atom Transfer Radical Polymerization: Experimental and Computational Studies. *J. Am. Chem. Soc.* **2016**, *138*, 2411−2425.
(37) Tang, W.; Matyjaszewski, K. Effects of Initiator Structure on Activation Rate Constants in ATRP. *Macromolecules* **2007**, *40*, 1858−1863.
(38) Horn, M.; Matyjaszewski, K. Solvent Effects on the Activation Rate Constant in Atom Transfer Radical Polymerization. *Macromolecules* **2013**, *46*, 3350−3357.
(39) Gillies, M. B.; Matyjaszewski, K.; Norrby, P.-O.; Pintauer, T.; Poli, R.; Richard, P. A DFT Study of R−X Bond Dissociation Enthalpies of Relevance to the Initiation Process of Atom Transfer Radical Polymerization. *Macromolecules* **2003**, *36*, 8551−8559.
(40) Koyama, D.; Dale, H. J. A.; Orr-Ewing, A. J. Ultrafast Observation of a Photoredox Reaction Mechanism: Photoinitiation in Organocatalyzed Atom-Transfer Radical Polymerization. *J. Am. Chem. Soc.* **2018**, *140*, 1285−1293.
(41) Jockusch, S.; Yagci, Y. The Active Role of Excited States of Phenothiazines in Photoinduced Metal Free Atom Transfer Radical Polymerization: Singlet or Triplet Excited States? *Polym. Chem.* **2016**, *7*, 6039−6043.
(42) Turro, N. J. Modern Molecular Photochemistry, 1st ed.; University Science Books: Sausalito, CA, 1991.
(43) Sartor, S. M.; McCarthy, B. G.; Pearson, R. M.; Miyake, G. M.; Damrauer, N. H. Exploiting Charge-Transfer States for Maximizing Intersystem Crossing Yields in Organic Photoredox Catalysts. *J. Am. Chem. Soc.* **2018**, *140*, 4778−4781.
(44) Sartor, S. M.; Lattke, Y. M.; McCarthy, B. G.; Miyake, G. M.; Damrauer, N. H. Effects of Naphthyl Connectivity on the Photophysics of Compact Organic Charge-Transfer Photoredox Catalysts. *J. Phys. Chem. A* **2019**, *123*, 4727−4736.
(45) van Willigen, H.; Jones, G.; Farahat, M. S. Time-Resolved EPR Study of Photoexcited Triplet-State Formation in Electron-Donor-Substituted Acridinium Ions. *J. Phys. Chem. B* **1996**, *100*, 3312−3316.
(46) Okada, T.; Karaki, I.; Matsuzawa, E.; Mataga, N.; Sakata, Y.; Misumi, S. Ultrafast Intersystem Crossing in Some Intramolecular Heteroexcimers. *J. Phys. Chem. A* **1981**, *85*, 3957−3960.
(47) Kim, H.; Scholes, G. D. Configuration Mixing upon Reorganization of Dihedral Angle Induces Rapid Intersystem Crossing in Organic Photoredox Catalyst. *Phys. Chem. Chem. Phys.* **2020**, *22*, 13292−13298.
(48) Lim, C.-H.; Ryan, M. D.; McCarthy, B. G.; Theriot, J. C.; Sartor, S. M.; Damrauer, N. H.; Musgrave, C. B.; Miyake, G. M. Intramolecular Charge Transfer and Ion Pairing in N,N-Diaryl Dihydrophenazine Photoredox Catalysts for Efficient Organocatalyzed Atom Transfer Radical Polymerization. *J. Am. Chem. Soc.* **2017**, *139*, 348−355.
(49) Lakowicz, J. R. *Principles of Fluorescence Spectroscopy*; Springer, 2013.
(50) Eberson, L. *Electron Transfers in Organic Chemistry*; Springer-Verlag, 1987.
(51) Kavarnos, G. J. *Fundamentals of Photoinduced Electron Transfer*; VCH Publishers: New York, 1993.
(52) Cannon, R. D. *Electron Transfer Reactions*; Butterworth, 1980.
(53) Arceo, E.; Montroni, E.; Melchiorre, P. Photo-Organocatalysis of Atom-Transfer Radical Additions to Alkenes. *Angew. Chem., Int. Ed.* **2014**, *53*, 12064−12068.
(54) Luo, Y.-R. *Handbook of Bond Dissociation Energies in Organic Compounds*; CRC Press, 2002.
(55) Nain, A. K. Densities, Ultrasonic Speeds, Viscosities and Excess Properties of Binary Mixtures of Methyl Methacrylate with N,N-Dimethylformamide and N,N-Dimethylacetamide at Different Temperatures. *J. Chem. Thermodyn.* **2013**, *60*, 105−116.
(56) Eberson, L.; et al. Electron Transfer Reactions in Organic Chemistry. II. An Analysis of Alkyl Halide Reduction by Electron Transfer Reagents on the Basis of the Marcus Theory. *Acta Chem. Scand., Ser. B* **1982**, *36*, 533−543.
(57) Saveant, J. M. A Simple Model for the Kinetics of Dissociative Electron Transfer in Polar Solvents. Application to the Homogeneous and Heterogeneous Reduction of Alkyl Halides. *J. Am. Chem. Soc.* **1987**, *109*, 6788−6795.
(58) Andrieux, C. P.; Le Gorande, A.; Saveant, J. M. Electron Transfer and Bond Breaking. Examples of Passage from a Sequential to a Concerted Mechanism in the Electrochemical Reductive Cleavage of Arylmethyl Halides. *J. Am. Chem. Soc.* **1992**, *114*, 6892−6904.
(59) Saveant, J. M. Electron Transfer, Bond Breaking, and Bond Formation. *Acc. Chem. Res.* **1993**, *26*, 455−461.
(60) Rehm, D.; Weller, A. Kinetics of Fluorescence Quenching by Electron and H-Atom Transfer. *Isr. J. Chem.* **1970**, *8*, 259−271.
(61) Pause, L.; Robert, M.; Savéant, J. Quantum Yields Lower than Unity in Photo-induced Dissociative Electron Transfers: The Reductive Cleavage of Carbon Tetrachloride. *ChemPhysChem* **2000**, *1*, 199−205.

https://doi.org/10.1021/acs.jpca.1c00855
J. Phys. Chem. A 2021, 125, 3109−3121

(62) Turró, C.; Zaleski, J. M.; Karabatsos, Y. M.; Nocera, D. G. Bimolecular Electron Transfer in the Marcus Inverted Region. *J. Am. Chem. Soc.* **1996**, *118*, 6060−6067.
(63) Murov, S. L.; Carmichael, I.; Hug, G. *Handbook of Photochemistry*; Marcel Dekker, Inc: New York, 1993; pp 298−304.
(64) Zepp, R. G. Quantum Yields for Reaction of Pollutants in Dilute Aqueous Solution. *Environ. Sci. Technol.* **1978**, *12*, 327−329.
(65) Zepp, R. G.; Cline, D. M. Rates of Direct Photolysis in Aquatic Environment. *Environ. Sci. Technol.* **1977**, *11*, 359−366.

https://doi.org/10.1021/acs.jpca.1c00855
J. Phys. Chem. A 2021, 125, 3109−3121